

# *7. Structural modifications of $Gd_2Zr_2O_7$ pyrochlore induced by swift heavy ions for nuclear waste immobilization*

## **7.1 Introduction**

The multifarious types of radioactive wastes are generated at different stages of the nuclear power industry [1]. The safe and effective management of high-level radioactive wastes (HLW) is of utmost importance. The borosilicate glasses are enormously used as a host matrix for the immobilization of high-level radioactive nuclides [2].

However, the metastable nature of the material is a major concern for such types of matrices. Moreover, under an accidental scenario, ingress of water into glass matrices can cause the development of water-soluble salts and results in, enrich the propensity of leachability of certain immobilized constituents [2]. Therefore, presently, the ceramics matrices are considered a suitable candidate for the immobilization of radioactive nuclides. Ceramic matrices have numerous advantages such as lower leaching rate, high radiation tolerance, high chemical, and thermal stability which are inevitable parameters for the immobilization of radioactive nuclides [3].

Among the several ceramics, the pyrochlore compounds have been reflected as a potential candidate for the safe and effective management of radioactive nuclides because of complex crystal structures that ease the accommodation of diverse actinides at crystallographic sites [4]. The enormous radiation tolerance studies of pyrochlore compounds for possible use in hostile environments such as nuclear reactors or immobilization of radioactive waste have been investigated previously [4–8]. Pyrochlore compounds with dissimilar cation radii cannot easily favor the O-D (order-disorder) transition and result in, pyrochlore structure leading to amorphization upon ion irradiation [4].

However, pyrochlore compounds with analogous cation radii easily form antisite defects and favor the O-D transformation upon irradiation [6]. Amongst the zirconate pyrochlores,  $Gd_2Zr_2O_7$  (GZO) is considered to be suitable host material for radioactive radionuclides. The reason for this is that the GZO lies on the boundary of pyrochlore and defect-fluorite structure having an ionic radius of 1.46 and easily forms an order-disorder instead of being amorphized upon ion irradiation [5].

The swift heavy ion irradiation induced amorphization and phase transformation from ordered pyrochlore to defect fluorite structure (O-D transformation) strongly depend on their chemical

composition, irradiation temperature, ion energy, and fluence [6,9–12]. Notably, the pyrochlore structure displays an extensive range of performance in response to ion irradiation, i.e., pyrochlore structure becomes amorphous or converts into defect fluorite structure i.e. a highly radiation-resistant phase [10,11].

Moreover, the GZO system demonstrated superior radiation resistance characteristics because of having a natural tendency to accommodate lattice disorder [13].

Therefore, the evaluation of phase transformation with the augmentation of fluence is important for the possible use of the materials in hostile environments. In this chapter, we have explored the role of ion fluence on the phase transformation of GZO. The synthesis and irradiation process of GZO samples is described in the respective section of chapter 2.

## **7.2. Results and Discussion**

### **7.2.1 Phase and microstructure analysis of pristine GZO**

To examine the phase and crystal structure of the GZO sample, the XRD pattern of the pristine GZO sample was recorded as displayed in Fig. 7.1 (a). It exhibits two different series of diffraction peaks, the first series that contains high-intensity peaks with the even Miller indices, i.e., (222), (400), and (440) represents the parent fluorite structure. The second series with weak intensity as marked with odd Miller indices, i.e., (111), (311) and (331), (511), and (531) corresponds to the ordered  $A_2B_2O_7$  pyrochlore superstructure (as marked with an asterisk ‘\*’) [11]. Thus, the presence of superstructure reflections in the XRD pattern of the pristine GZO sample confirmed the formation of the ordered pyrochlore phase [Fig. 7.1 (a)]. The intensity of various reflections is strongly associated with the scattering power of cations that occupy two distinct A and B sites. It should be noted that in the XRD patterns, the influence of cations is predominant because the scattering power is relatively lower for oxygen atoms than cations [14].

The crystallite size and lattice strain were deduced from Williamson- Hall (W-H) plot [15] as displayed in Fig. 7.2 (b). The calculated crystallite size and lattice strain of the pristine GZO are found to be 86.09 nm and 0.106 %, respectively. To get more insight into the crystal structure and unit cell parameter, Rietveld refinement was executed on the diffraction patterns of pristine GZO sample using the Fullprof program [16]. Fig. 7.1 (c) shows the Rietveld refinement of the diffraction patterns of the pristine GZO sample. Here, we wish to stress that the Rietveld refinement of the GZO sample exhibits that the GZO sample possesses an ordered

pyrochlore phase. The unit cell parameter of the GZO sample quantified from the Rietveld refinement is found to be 10.5438 (1) Å.

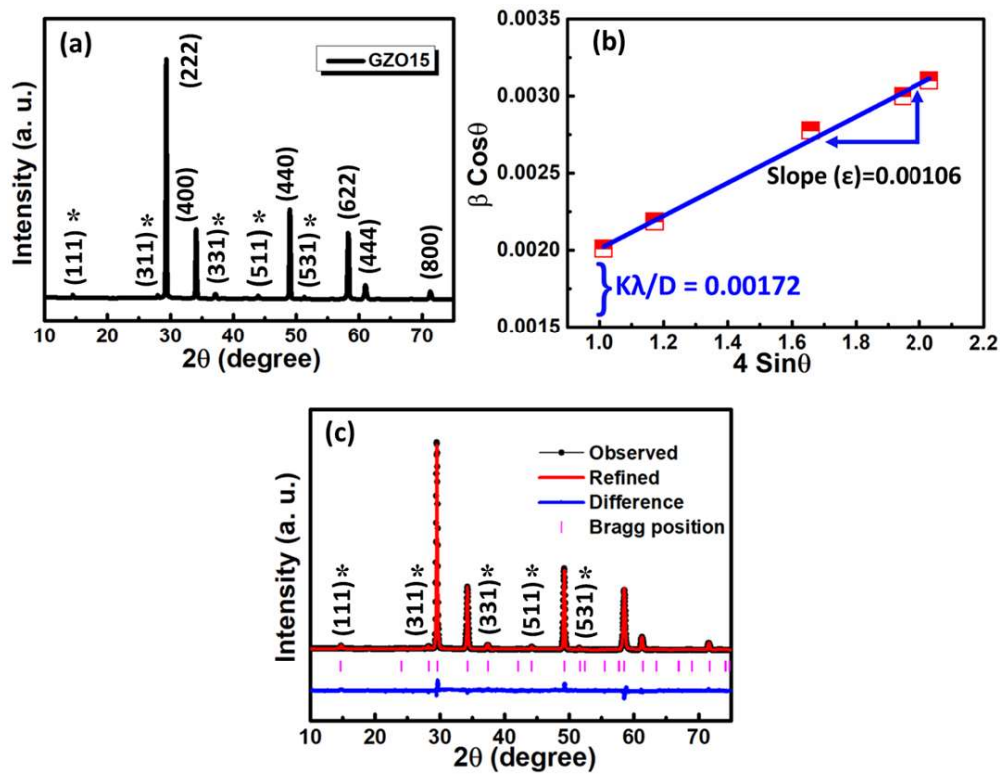


**Figure 7.1** XRD patterns (a), (b) W-H plot, and (c) Rietveld refinement of the pristine GZO sample. The superstructure reflections are marked with an asterisk (\*).

The previous studies reported that the unit cell parameter of the GZO lies in a similar range [2,17]. The theoretical density ( $\rho_{th}$ ) was calculated using the unit lattice parameter that was deduced from the Rietveld refinement of the powder XRD pattern of GZO employing the following expression [12].

$$\rho_{th} = \frac{8 \times 10^{24} M}{N_a a^3} \text{ g/cm}^3 \quad (7.1)$$

Where  $M$  represents the molecular weight (gm/mole),  $N_a$  represents the Avogadro number,  $6.02 \times 10^{23} \text{ mol}^{-1}$ , and  $a$  depicts the unit cell parameter.

The microstructure of the pristine sample was investigated by FE-SEM. Fig. 7.2 displays the FE-SEM image of the pre-irradiated GZO sample and grains size were quantified employing the rectangular intercept process [18]. The grains and grain boundaries are apparently visible which seems associated with the micrometer grain size. The calculated average grain is found to be  $2.82 \pm 0.21 \mu\text{m}$ .

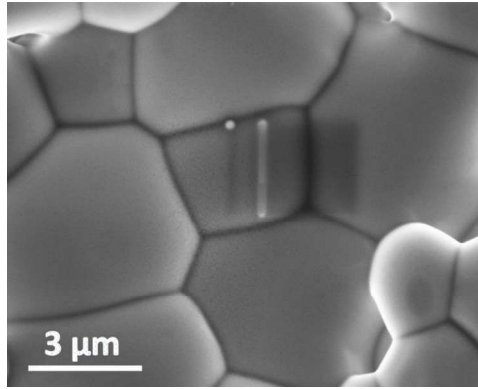


**Figure 7.2** FE-SEM micrograph of pristine GZO sample.

It is worth mentioning that the grain size determined from the FE-SEM is higher than that of size quantified from the XRD technique because the grains are composed of many crystallites and similar observation has been reported in earlier studies [18,19].

## **7.2.1 Radiation damage upon ion irradiation of 100 MeV I<sup>7+</sup> ions**

### **7.2.1.1 Structural modification analysis by XRD**

To explore the radiation tolerance of the GZO sample for hostile environments, the GZO samples were irradiated with the 100 MeV I<sup>7+</sup> ions at the fluence of  $1.0 \times 10^{12}$ ,  $3.0 \times 10^{12}$ ,  $1.0 \times 10^{13}$ ,  $3.0 \times 10^{13}$ ,  $1.0 \times 10^{14}$  ions/cm<sup>2</sup>. Fig. 7.3 exhibits the powder XRD patterns of before and after irradiation of the GZO sample as a function of ion fluence. Upon irradiation with swift heavy ion, no additional peaks and diffuse scattering were recorded in XRD patterns of irradiated GZO samples.

In the pyrochlore phase, the decrement in superstructure reflection intensity than theoretical intensity can be associated with either the existence of pyrochlore and fluorite phases or the occurrence of antisite defects in the system [8]. As per Lang et al. [10] and Begg et al., [20] the GZO sintered at 1600°C possesses nearly 65% of fluorite phase. In the present study, the GZO sample was annealed at 1500°C that lies below the O-D transition for GZO (~1530°C), and the longer heating duration ensures less disordering in the system as confirmed by the Rietveld refinement [14].

Fig. 7.3 shows that all the diffraction peaks slightly decrease with an increase of ion fluence, and peaks width also seem to be relatively broader upon irradiation of 100 MeV iodine ions [5]. The superstructure reflections corresponding to the pyrochlore phase structure are marked with the asterisk ‘\*’ as illustrated in Fig. 7.3.

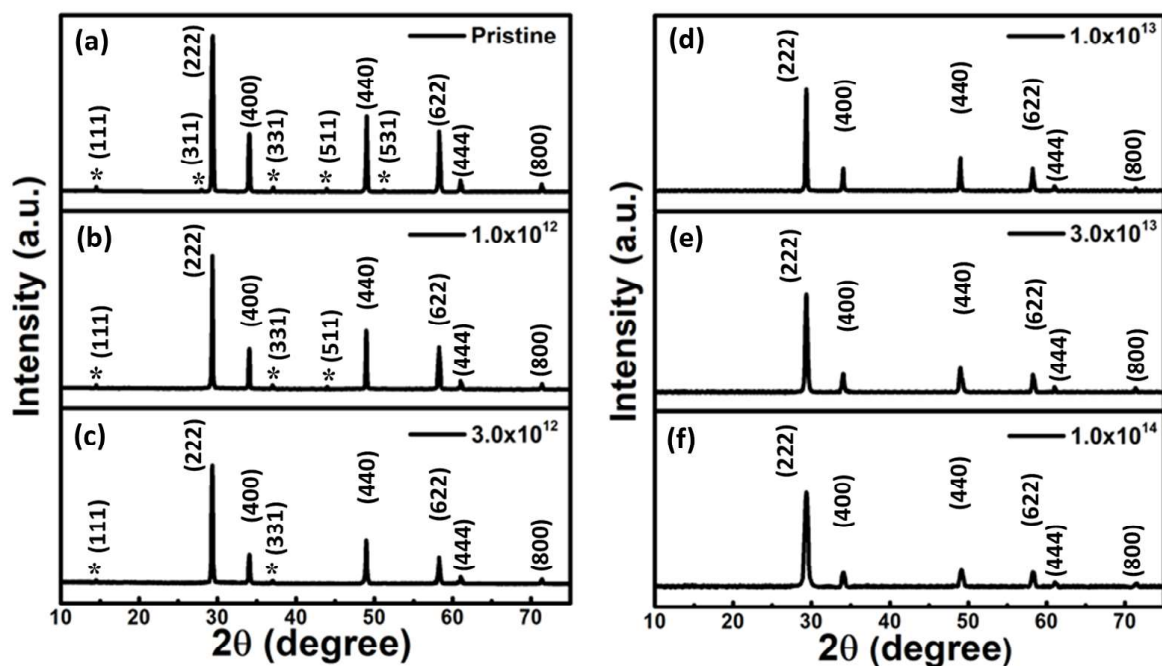


**Figure 7.3** XRD patterns of GZO sample before and after irradiation with 100 MeV  $I^{7+}$  ions as a function of ion fluence.

Sattonnay et al. irradiated the GZO samples using swift heavy ions (870 MeV Xe) at various fluence. They found that the intensity of the superstructure reflections decreases with the increase of ion fluence due to enhanced disorder upon irradiation [14]. In a similar way, the superstructure reflections that belong to the pyrochlore phase structure are being disappeared as a function of ion fluence [Fig. 7.3 (d-f)]. The sample irradiated with the fluence of  $1.0 \times 10^{12}$  ions/cm<sup>2</sup> exhibits superstructure reflections, i.e., (111), (311), and 511) which is in well agreement with the previous results [21]. Moreover, Sattonnay et al. stated that the pyrochlore superstructure ordering remained intact upon irradiation of 870 MeV Xe ions at the ion fluence of  $1.0 \times 10^{12}$  ions/cm<sup>2</sup> [14].

Recently, Kumar et al. reported that the GZO preserved the superstructure pyrochlore phase upon irradiation of 120 MeV  $Au^{9+}$  ions at the ion fluence of  $5.0 \times 10^{12}$  ions/cm<sup>2</sup> [11]. Here, we would like to emphasize that the XRD pattern of the GZO irradiated at the fluence of  $3.0 \times 10^{12}$  ions/cm<sup>2</sup> demonstrates the appearance of (111) and (331) superstructure reflection, which suggest that the GZO sample preserved the pyrochlore structure. GZO sample irradiated at the fluence of  $1.0 \times 10^{13}$  ions/cm<sup>2</sup> demonstrates the only reflections related to the fluorite structure. Further, it is worth mentioning that we have not observed the signature of amorphization in GZO sample irradiated at the higher fluences ( $3.0 \times 10^{13}$  ions/cm<sup>2</sup> to  $1.0 \times 10^{14}$  ions/cm<sup>2</sup>), i.e., the GZO sample demonstrates the pyrochlore to fluorite structure phase

transition upon irradiation at the highest ion fluence. The relative peak broadening at higher fluence suggests ion irradiation-induced order-disorder transformation, i.e., GZO sample converts into the disordered defect fluorite ( $Fm\bar{3}m$ ) phase on account of disordering in the occupancies of the Gd and Zr cations at both A and B sites [5,10,11,14,21]. Here, it should be noted that no signal of amorphization was perceived in the GZO system even at the highest ion fluence of  $1.0 \times 10^{14}$  ions/cm<sup>2</sup> which established the capabilities of GZO for possible applications in hostile environments such as immobilization of high-level radioactive waste nuclides.

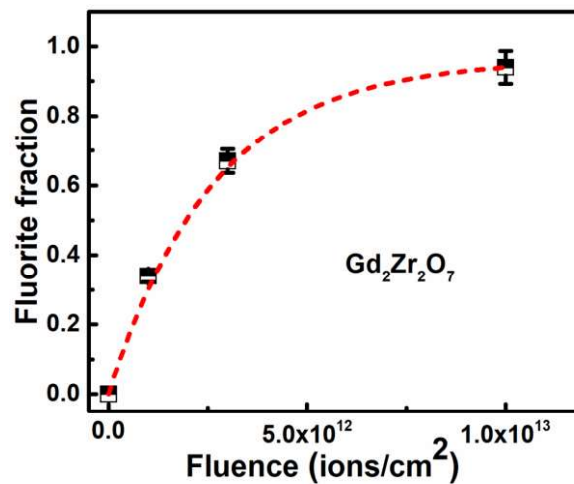


**Figure 7.4** Variation of fluorite phase fraction as a function of ion fluence irradiated with 100 MeV  $I^{7+}$  ions.

We wish to emphasize that the electronic excitation caused by the slowing-down of swift heavy ions in ceramic matrices favored the production of ion tracks, called cylindrical damaged zones [21]. Fig. 7.4 exhibits the fluorite phase fraction as a function of ion fluence that is quantified from the XRD patterns of GZO samples. The fluorite phase fraction increases with the enhancement of ion fluence (Fig. 7.4) and it shows the nearly complete phase transformation (pyrochlore to fluorite phase) upon irradiation at the ion fluence of  $1.0 \times 10^{13}$  ions/cm<sup>2</sup>. In the direct impact model, the phase transformation is governed by the ion impinging into an undamaged region (It is commonly assumed that a single collision is enough to transform the system within the ion track) [21]. The fluorite fraction as a function of ion fluence was fitted using the equation described well by the direct-impact model as follows [22,23].

$$f_a = f_o [1 - \exp(-\alpha\eta)] \quad (7.2)$$

Where  $f_o$  is the maximum transformed fraction (at high fluence) and  $f_a = 1$  represents the complete phase transformation,  $\alpha$  is the phase transformation cross-section, and  $\eta$  is the ion fluence. The tracks were assumed to be in cylindrical dimensions in the compounds and the

quantified cross-section area through the experimental data fitting was found to be  $48.11 \pm 34 \text{ nm}^2$ , respectively. The diameter of ion tracks ( $d$ ) was deduced using the expression,  $d = 2(\sigma_i/\pi)^{1/2}$  [21] and it is found to be  $7.82 \pm 0.32 \text{ nm}$ . The calculated cross-section area and ion track radius values for the GZO system are in well agreement with those previously observed upon irradiation of 90 MeV Xe ions and 120 MeV Au ions, respectively [11,21].

Here, it should be noted that the GZO system demonstrates order-disorder, i.e., pyrochlore to fluorite phase transformation at the ion fluence of  $1.0 \times 10^{13} \text{ ions/cm}^2$  and no amorphization was observed in the GZO samples. The pyrochlore to fluorite phase transformation characteristics upon ion irradiation signifies the capability of prepared GZO samples for the immobilization of radioactive nuclides.

### 7.2.1.2 Analysis of vibrational modes by Raman spectroscopy

Raman spectroscopy is used to examine the structural defects in the pyrochlore matrices [17]. Therefore, Raman spectroscopy was performed to get more insight into order-disorder transformation upon irradiation of 100 MeV iodine ions. It is noteworthy that Raman spectroscopy is highly sensitive to metal-oxygen vibrational modes whereas XRD is the most suitable technique to determine the cations disorder [17].

According to the earlier studies, the vibrational properties of  $A_2B_2O_7$  compounds depend on the specific compositions [5,6,10,14,24]. Factor group analysis and theoretical calculations [2,17,25–28] on  $A_2B_2O_7$  compounds revealed that the pyrochlore phase has six Raman active modes ( $A_{1g} + E_g + 4F_{2g}$ ) and defect fluorite structure possesses only a single Raman mode, i.e.,  $F_{2g}$  vibrational mode.

Fig. 7.5 (a-f) displays the Raman spectra of before and after irradiation GZO samples at different fluences, i.e.,  $1.0 \times 10^{12}$ ,  $3.0 \times 10^{12}$ ,  $1.0 \times 10^{13}$ ,  $3.0 \times 10^{13}$ ,  $1.0 \times 10^{14} \text{ ions/cm}^2$  (please note the corresponding XRD patterns shown in Fig. 7.3). The Raman spectra of before irradiated LZO samples [Fig. 7.5 (a)] exhibits the appearance of four vibrational modes situated at  $\sim 319 \text{ cm}^{-1}$  ( $E_g$ ),  $406 \text{ cm}^{-1}$  ( $F_{2g}(1)$ ),  $532 \text{ cm}^{-1}$  ( $A_g$ ), and  $603 \text{ cm}^{-1}$  ( $F_{2g}(2)$ ). It is reported that the Raman bands in the pyrochlore compounds emerged merely from the anion sub-lattice vibrations, whereas in fluorite structure, emerged from the relative movements of the anions against fixed cations [28]. In the present study, Raman modes have been assigned by comparison with earlier reported pyrochlore structured materials [29,30].

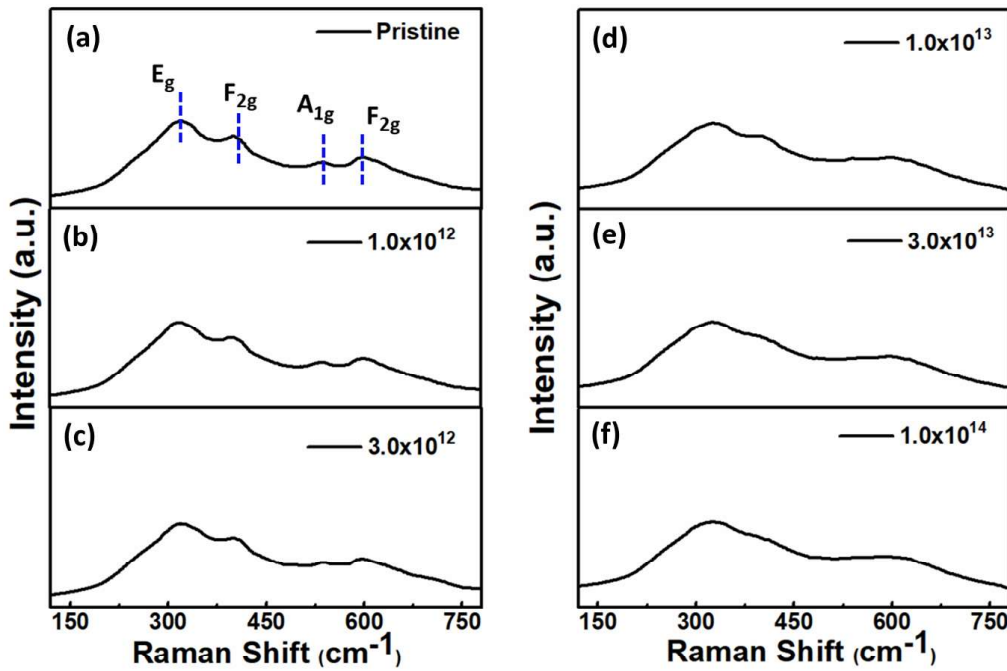


**Figure 7.5** Raman spectra of pristine and post irradiated GZO samples.

It is widely reported that the  $A_{1g}$ ,  $E_g$ , and three  $F_{2g}$  modes are typically associated with the vibration of the  $BO_6$  octahedra of the pyrochlore phase [25,31,32]. It is noteworthy that the lower wavenumber region mode, i.e.,  $E_g$  mode is generally associated with the O-B-O bending vibrations [17]. Brown et al. [30] stated that the vibrational mode,  $A_{1g}$ , also originated from the O-B-O bending vibrations. The  $F_{2g}$  modes originate from the contribution of B-O bond stretching and bending vibrations, and  $O_{(1)}-A-O_{(2)}$  bending vibrations [17,30].

It should be noted that several previous studies have reported the presence of four bands out of six bands in the respective Raman spectra [25,28] and two other possible Raman vibrational modes are difficult to resolve from the background [17]. Apart from these, previous studies have been reported a broad mode between  $650\text{ cm}^{-1}$  to  $780\text{ cm}^{-1}$ , and the origin of this mode is still under debate [2,10,33] and assume that it could be associated with the second-order Raman scattering [14,27]. According to earlier studies [14,17,27] the Raman active vibrational mode situated at  $319\text{ cm}^{-1}$  was assigned as  $E_g$  mode and two other vibrational modes at  $406\text{ cm}^{-1}$  and  $603\text{ cm}^{-1}$  were assigned as  $F_{2g}$  modes whereas the Raman vibrational band at  $532\text{ cm}^{-1}$  was referred as  $A_{1g}$  mode [Fig. 7.6]. It should be noted that the concurrently broadening and weakening in the respective Raman modes were observed with the enhancement of the ion fluence [Fig. 7.5]. This observation is found to be in well agreement with earlier studies [10,14]. The enhancement of ion fluence leads to an overlap of two weaker vibrational modes ( $532$  and  $603\text{ cm}^{-1}$ ).

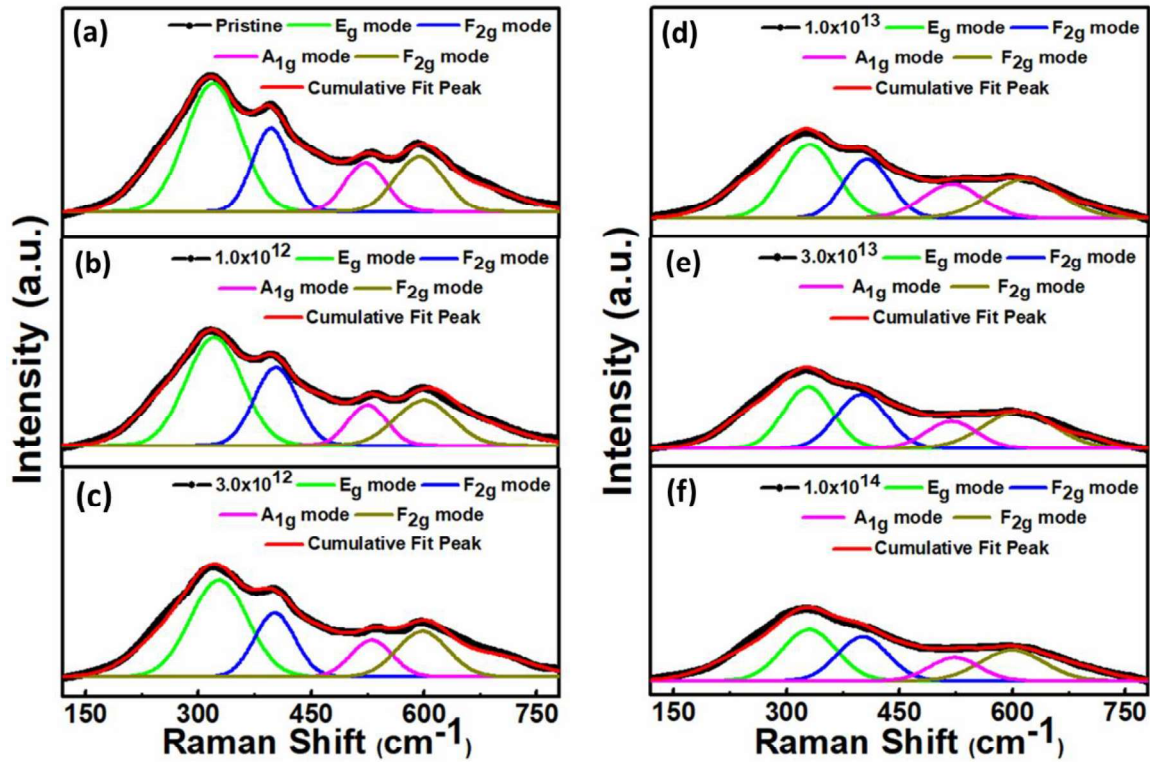


**Figure 7.6** Deconvoluted Raman spectra of pristine and post irradiated GZO samples.

Upon ion irradiation, enhancement in the peak broadening and decrement in the intensity with the increase of ion fluence, indicating a significant loss of crystallinity, local disordering, and distortion of chemical bonds [10,14].

It is worth mentioning that for the fluorite structure ( $Fm\bar{3}m$ ), only single vibrational Raman mode is active. In the case of defect fluorite structure, the selection rule is broken due to cation antisite defects (cation disordering) and vacancies in the oxygen sub-lattices [14]. Patel et al. stated that the ion irradiation induced the broadening in the vibrational band due to deterioration of ordering [6]. The vibrational band,  $A_{1g}$ , attributed to the Gd-O stretching mode almost disappears due to the emergence of pronounced deterioration, which suggests O-D transformation [6].

Lang et al. [10] reported the broadening and weakening in the vibrational modes with the increase of ion fluence upon irradiation of swift heavy 1.43 GeV Xe ions. They stated that the swift heavy (1.43 GeV Xe) ion irradiation deteriorates the chemical bonding in the respective vibrational bonds, which signifies the O-D phase transformation in the system. In the present study, the Raman spectra of irradiated GZO samples exhibit peak broadening and weakening as a function of ion fluence which indicates O-D transition [Fig. 7.5], i.e., the phase transformation from pyrochlore to fluorite structure. The irradiated GZO samples with the

increase of fluence did not exhibit any evidence of amorphization in Raman spectra which is well corroborated with the XRD results.

Moreover, it is typically complicated to quantify the reliable broadening and weakening in the respective vibrational modes, because the ion irradiation augments the background. The broadening and weakening in vibrational modes can be analyzed with the help of the peak fitting procedure. Therefore, Raman spectra recorded before and after irradiation were fitted using the Gaussian function. During the fitting procedure, the peak position, intensity, and width of the peaks were kept as free fitting parameters. Deconvoluted Raman spectra of before and after irradiated (irradiated at different fluences, i.e.,  $1.0 \times 10^{12}$  to  $1.0 \times 10^{14}$  ions/cm<sup>2</sup>) GZO samples are presented in Fig. 7.6.

Deconvoluted Raman spectra of all samples suggest that the FWHM of the Raman modes increases and intensity decreases with the augmentation of ion fluence [Fig. 7.6]. The presence of weak and broad characteristics in the Raman spectra exhibits the presence of subtle pyrochlore type ordering irrespective of the extent of disorder upon ion irradiation [5]. The pyrochlore and fluorite matrices are associated with the extent of degrees of disordering of cations and anions/vacancies in the respective sub-lattices. The augmented disorder in cation and anion sub-lattices transforms the system from pyrochlore → defect pyrochlore → defect fluorite hierarchy [5].

The GZO lies on the boundary of the pyrochlore-defect-fluorite phase structure because of its cationic ratio, 1.46. Therefore, GZO is considered defective pyrochlore due to the presence of cation antisite defects and disordering of anions/vacancies [8]. Further, it is reported that the disordering in the GZO system is enriched with augmentation of ion fluence which gives rise to the appearance of broadening and weakening in Raman modes. Kumari et al. reported that the pyrochlore GZO transforms into the defect fluorite-type structure with the weak pyrochlore-type ordering upon irradiation of 120 MeV Au ion at the fluence of  $1.0 \times 10^{14}$  ions/cm<sup>2</sup> [5].

Here, we wish to stress that the Raman spectra of GZO samples [Fig. 7.5 and Fig. 7.6] show the weakening and broadening of vibrational modes with ion fluence. This result specifies that ion irradiation induces disorder/distortion in the respective vibrational modes and it enhances with the increase of fluence, i.e., the vibrational modes deteriorate with the function of fluence. The GZO samples irradiated with the fluence of  $3.0 \times 10^{13}$  ions/cm<sup>2</sup> and  $1.0 \times 10^{14}$  ions/cm<sup>2</sup> can be defined as having weakly ordered pyrochlore ordering with a bulk defect-fluorite structure upon ion irradiation [Fig. 7.5 (f) and Fig. 7.6 (f)] [5].

Therefore, we conclude that the Raman spectroscopy results of GZO samples strengthen the XRD results and demonstrate pyrochlore-fluorite phase transition upon ion irradiation. The characteristics of the GZO sample, i.e., pyrochlore to fluorite phase transformation demonstrate the competence of the GZO samples for applications in hostile environments.

### 7.3 Conclusion

The GZO samples were irradiated using 100 MeV  $I^{7+}$  ions and the impact of ion fluence on the structural modifications for possible use in nuclear applications was explored. The two complementary analytical techniques, i.e., XRD and Raman spectroscopy were employed to examine the radiation-induced structural modifications (O-D transformation). The Rietveld refinement of the pristine GZO sample exhibited that the GZO has ordered pyrochlore structure as a major phase. XRD results analysis confirmed the irradiation induced structural modifications, i.e., pyrochlore to defect fluorite phase transition in GZO ceramics, and found to be ion fluence dependent. Specifically, the GZO samples irradiated for initial fluences ( $1.0 \times 10^{12}$  ions/cm<sup>2</sup> and  $3.0 \times 10^{12}$  ions/cm<sup>2</sup>) present the least degree of phase fraction. The Raman spectroscopy analysis also confirms the order-disorder in GZO samples. The degree of the disorder is enhanced as a function of ion fluence and disregards the appearance of amorphization. The pyrochlore to defect fluorite phase transformation without any signature of amorphization, even for the higher fluences, establishes the potentiality of GZO samples for utilization in nuclear applications as radioactive waste forms.

## References

- [1] K. Liu, K. Zhang, T. Deng, J. Zeng, B. Luo, H. Zhang, Grain size effects on the aqueous durability of  $Gd_2Zr_2O_7$  ceramics as high-level radioactive wastes matrix and its leaching mechanism, *Ceram. Int.* (2021) 1–11. <https://doi.org/10.1016/j.ceramint.2021.01.193>.
- [2] M. Jafar, S.B. Phapale, B.P. Mandal, M. Roy, S.N. Achary, R. Mishra, A.K. Tyagi, Effect of temperature on phase evolution in  $Gd_2Zr_2O_7$ : A potential matrix for nuclear waste immobilization, *J. Alloys Compd.* 867 (2021) 159032. <https://doi.org/10.1016/j.jallcom.2021.159032>.
- [3] M. Jafar, S.B. Phapale, B.P. Mandal, R. Mishra, A.K. Tyagi, Preparation and Structure of Uranium-Incorporated  $Gd_2Zr_2O_7$  Compounds and Their Thermodynamic Stabilities under Oxidizing and Reducing Conditions, *Inorg. Chem.* 54 (2015) 9447–9457. <https://doi.org/10.1021/acs.inorgchem.5b01300>.
- [4] C.A. Taylor, M.K. Patel, J.A. Aguiar, Y. Zhang, M.L. Crespillo, J. Wen, H. Xue, Y. Wang, W.J. Weber, Bubble formation and lattice parameter changes resulting from He irradiation of defect-fluorite  $Gd_2Zr_2O_7$ , *Acta Mater.* 115 (2016) 115–122. <https://doi.org/10.1016/j.actamat.2016.05.045>.
- [5] R. Kumari, P.K. Kulriya, V. Grover, R. Shukla, K. Saravanan, S. Mohapatra, A.K. Tyagi, D.K. Avasthi, Radiation stability of  $Gd_2Zr_2O_7$ : Effect of stoichiometry and structure, *Ceram. Int.* 42 (2016) 103–109. <https://doi.org/10.1016/j.ceramint.2015.08.007>.
- [6] M.K. Patel, V. Vijayakumar, D.K. Avasthi, S. Kailas, J.C. Pivin, V. Grover, B.P. Mandal, A.K. Tyagi, Effect of swift heavy ion irradiation in pyrochlores, *Nucl. Instruments Methods Phys. Res. Sect. B Beam Interact. with Mater. Atoms.* 266 (2008) 2898–2901. <https://doi.org/10.1016/j.nimb.2008.03.135>.
- [7] K. Liu, K. Zhang, T. Deng, W. Li, H. Zhang, Comparative study of irradiation effects on nanosized and microsized  $Gd_2Zr_2O_7$  ceramics, *Ceram. Int.* 46 (2020) 16987–16992. <https://doi.org/10.1016/j.ceramint.2020.03.283>.
- [8] R.C. Ewing, W.J. Weber, J. Lian, Nuclear waste disposal—pyrochlore ( $A_2B_2O_7$ ): Nuclear waste form for the immobilization of plutonium and “minor” actinides, *J. Appl. Phys.* 95 (2004) 5949–5971. <https://doi.org/10.1063/1.1707213>.
- [9] M.K. Patel, V. Vijayakumar, S. Kailas, D.K. Avasthi, J.C. Pivin, A.K. Tyagi, Structural modifications in pyrochlores caused by ions in the electronic stopping regime, *J. Nucl. Mater.* 380 (2008) 93–98. <https://doi.org/10.1016/j.jnucmat.2008.07.007>.

- [10] M. Lang, F.X. Zhang, R.C. Ewing, J. Lian, C. Trautmann, Z. Wang, Structural modifications of  $\text{Gd}_2\text{Zr}_{2-x}\text{Ti}_x\text{O}_7$  pyrochlore induced by swift heavy ions: Disordering and amorphization, *J. Mater. Res.* 24 (2009) 1322–1334. <https://doi.org/10.1557/jmr.2009.0151>.
- [11] A. Kumar, P.K. Kulriya, S.K. Sharma, V. Grover, A.K. Tyagi, V.K. Shukla, Structural and compositional effects on the electronic excitation induced phase transformations in  $\text{Gd}_2\text{Ti}_{2-y}\text{Zr}_y\text{O}_7$  pyrochlore, *J. Nucl. Mater.* 539 (2020). <https://doi.org/10.1016/j.jnucmat.2020.152278>.
- [12] A. Panghal, Y. Kumar, P.K. Kulriya, P.M. Shirage, N.L. Singh, Structural assessment and irradiation response of  $\text{La}_2\text{Zr}_2\text{O}_7$  pyrochlore: Impact of irradiation temperature and ion fluence, *J. Alloys Compd.* 862 (2021) 158556. <https://doi.org/10.1016/j.jallcom.2020.158556>.
- [13] K.E. Sickafus, R.W. Grimes, J.A. Valdez, A. Cleave, M. Tang, M. Ishimaru, S.M. Corish, C.R. Stanek, B.P. Uberuaga, Radiation-induced amorphization resistance and radiation tolerance in structurally related oxides, *Nat. Mater.* 6 (2007) 217–223. <https://doi.org/10.1038/nmat1842>.
- [14] G. Sattonnay, S. Moll, L. Thomé, C. Decorse, C. Legros, P. Simon, J. Jagielski, I. Jozwik, I. Monnet, Phase transformations induced by high electronic excitation in ion-irradiated  $\text{Gd}_2(\text{Zr}_x\text{Ti}_{1-x})_2\text{O}_7$  pyrochlores, *J. Appl. Phys.* 108 (2010) 103512. <https://doi.org/10.1063/1.3503452>.
- [15] Y. Kumar, A.K. Rana, P. Bhojane, M. Pusty, V. Bagwe, S. Sen, P.M. Shirage, Controlling of ZnO nanostructures by solute concentration and its effect on growth, structural and optical properties, *Mater. Res. Express.* 2 (2015) 105017. <https://doi.org/10.1088/2053-1591/2/10/105017>.
- [16] Y. Kumar, A. Sharma, M.A. Ahmed, S.S. Mali, C.K. Hong, P.M. Shirage, Morphology-controlled synthesis and enhanced energy product (BH) max of  $\text{CoFe}_2\text{O}_4$  nanoparticles, *New J. Chem.* 42 (2018) 15793–15802. <https://doi.org/10.1039/C8NJ02177E>.
- [17] L. Kong, I. Karatchevtseva, D.J. Gregg, M.G. Blackford, R. Holmes, G. Triani,  $\text{Gd}_2\text{Zr}_2\text{O}_7$  and  $\text{Nd}_2\text{Zr}_2\text{O}_7$  pyrochlore prepared by aqueous chemical synthesis, *J. Eur. Ceram. Soc.* 33 (2013) 3273–3285. <https://doi.org/10.1016/j.jeurceramsoc.2013.05.011>.
- [18] A. Panghal, P.K. Kulriya, Y. Kumar, F. Singh, N.L. Singh, Investigations of atomic disorder and grain growth kinetics in polycrystalline  $\text{La}_2\text{Zr}_2\text{O}_7$ , *Appl. Phys. A Mater. Sci. Process.* 125 (2019) 1–11. <https://doi.org/10.1007/s00339-019-2720-8>.
- [19] C. Kaliyaperumal, A. Sankarakumar, T. Paramasivam, Grain size effect on the electrical

- properties of nanocrystalline  $Gd_2Zr_2O_7$  ceramics, *J. Alloys Compd.* 813 (2020). <https://doi.org/10.1016/j.jallcom.2019.152221>.
- [20] S.X. Wang, B.D. Begg, L.M. Wang, R.C. Ewing, W.J. Weber, K. V. Govidan Kutty, Radiation stability of gadolinium zirconate: A waste form for plutonium disposition, *J. Mater. Res.* 14 (1999) 4470–4473. <https://doi.org/10.1557/JMR.1999.0606>.
- [21] G. Sattonnay, L. Thomé, N. Sellami, I. Monnet, C. Grygiel, C. Legros, R. Tetot, Phase transformations in pyrochlores irradiated with swift heavy ions: Influence of composition and chemical bonding, *Acta Phys. Pol. A.* 123 (2013) 862–866. <https://doi.org/10.12693/APhysPolA.123.862>.
- [22] J.F. Gibbons, Ion implantation in semiconductors—Part II: Damage production and annealing, *Proc. IEEE.* 60 (1972) 1062–1096. <https://doi.org/10.1109/PROC.1972.8854>.
- [23] W.J. Weber, Models and mechanisms of irradiation-induced amorphization in ceramics, *Nucl. Instruments Methods Phys. Res. Sect. B Beam Interact. with Mater. Atoms.* 166 (2000) 98–106. [https://doi.org/10.1016/S0168-583X\(99\)00643-6](https://doi.org/10.1016/S0168-583X(99)00643-6).
- [24] Q. Qing, X. Shu, D. Shao, H. Zhang, F. Chi, X. Lu, Irradiation response of  $Nd_2Zr_2O_7$  under heavy ions irradiation, *J. Eur. Ceram. Soc.* 38 (2018) 2068–2073. <https://doi.org/10.1016/j.jeurceramsoc.2017.11.050>.
- [25] D. Michel, M.P. y Jorba, R. Collongues, Study by Raman spectroscopy of order-disorder phenomena occurring in some binary oxides with fluorite-related structures, *J. Raman Spectrosc.* 5 (1976) 163–180. <https://doi.org/10.1002/jrs.1250050208>.
- [26] M. Glerup, O.F. Nielsen, F.W. Poulsen, The Structural Transformation from the Pyrochlore Structure,  $A_2B_2O_7$ , to the Fluorite Structure,  $AO_2$ , Studied by Raman Spectroscopy and Defect Chemistry Modeling, *J. Solid State Chem.* 160 (2001) 25–32. <https://doi.org/10.1006/jssc.2000.9142>.
- [27] B.P. Mandal, N. Garg, S.M. Sharma, A.K. Tyagi, Solubility of  $ThO_2$  in  $Gd_2Zr_2O_7$  pyrochlore: XRD, SEM and Raman spectroscopic studies, *J. Nucl. Mater.* 392 (2009) 95–99. <https://doi.org/10.1016/j.jnucmat.2009.03.050>.
- [28] B.E. SCHEETZ, W.B. WHITE, Characterization of Anion Disorder in Zirconate  $A_2B_2O_7$  Compounds by Raman Spectroscopy, *J. Am. Ceram. Soc.* 62 (1979) 468–470. <https://doi.org/10.1111/j.1151-2916.1979.tb19107.x>.
- [29] H.C. Gupta, J. Singh, S. Kumar, Karandeep, N. Rani, A lattice dynamical investigation of the Raman and the infrared frequencies of the  $Dy_2Ti_2O_7$  pyrochlore spin ice compound, *J. Mol. Struct.* 937 (2009) 136–138. <https://doi.org/10.1016/j.molstruc>.

2009.08.027.

- [30] S. Brown, H.C. Gupta, J.A. Alonso, M.J. Martinez-Lope, Vibrational spectra and force field calculation of  $A_2Mn_2O_7$  ( $A = Y, Dy, Er, Yb$ ) pyrochlores, *J. Raman Spectrosc.* 34 (2003) 240–243. <https://doi.org/10.1002/jrs.982>.
- [31] L. Zhou, Z. Huang, J. Qi, Z. Feng, D. Wu, W. Zhang, X. Yu, Y. Guan, X. Chen, L. Xie, K. Sun, T. Lu, Thermal-Driven Fluorite–Pyrochlore–Fluorite Phase Transitions of  $Gd_2Zr_2O_7$  Ceramics Probed in Large Range of Sintering Temperature, *Metall. Mater. Trans. A.* 47 (2016) 623–630. <https://doi.org/10.1007/s11661-015-3234-4>.
- [32] Y.H. Lee, H.S. Sheu, J.P. Deng, H.-C.I. Kao, Preparation and fluorite–pyrochlore phase transformation in  $Gd_2Zr_2O_7$ , *J. Alloys Compd.* 487 (2009) 595–598. <https://doi.org/10.1016/j.jallcom.2009.08.021>.
- [33] N.J. Hess, B.D. Begg, S.D. Conradson, D.E. McCready, P.L. Gassman, W.J. Weber, Spectroscopic Investigations of the Structural Phase Transition in  $Gd_2(Ti_{1-y}Zr_y)_2O_7$  Pyrochlores, *J. Phys. Chem. B.* 106 (2002) 4663–4677. <https://doi.org/10.1021/jp014285t>.